Spin Ground State and Magnetic Properties of Cobalt(II): Relativistic DFT Calculations Guided by EPR Measurements of Bis(2,4-acetylacetonate)cobalt(II)-Based Complexes

ARTICLE *in* THE JOURNAL OF PHYSICAL CHEMISTRY A · FEBRUARY 2011

Impact Factor: 2.69 · DOI: 10.1021/jp109524t · Source: PubMed

THE JOURNAL OF PHYSICAL CHEMISTRY A

ARTICLE

pubs.acs.org/JPCA

Spin Ground State and Magnetic Properties of Cobalt(II): Relativistic DFT Calculations Guided by EPR Measurements of Bis(2,4-acetylacetonate)cobalt(II)-Based Complexes

Piotr Pietrzyk,* Monika Srebro, Mariusz Radoń, Zbigniew Sojka, and Artur Michalak

Faculty of Chemistry, Jagiellonian University, ul. Ingardena 3, 30-060 Krakow, Poland

ABSTRACT: The spin ground state of the core ion and structure of the bis(2,4-acetylacetonate)cobalt(II) model complex and its synthetic aqua and ethanol derivatives, $Co(acac)_2L_n$, (L = EtOH, H_2O), were examined by means of density functional theory (DFT) calculations supported by electron paramagnetic resonance (EPR) measurements. Geometry optimizations were carried out for low-spin (doublet) and high-spin (quartet) states. For the $Co(acac)_2$ complex two possible conformations, a square-planar and a tetrahedral one, were taken into account. For all structures relative energies were calculated with both "pure" and hybrid functionals. The calculated data were complemented with the results of the EPR investigations carried out at liquid helium temperature, allowing for definite assignment of the high-spin state for the $Co(acac)_2(EtOH)_2$ complex. However, because of the unresolved spectral features, only effective *g*-values could be assessed, whereas the zero-field splitting parameters (ZFS) were calculated by means of the spin−orbit mean field (SOMF) relativistic DFT method for which direct spin−spin (SS) and spin−orbit coupling (SOC) contributions were quantified.

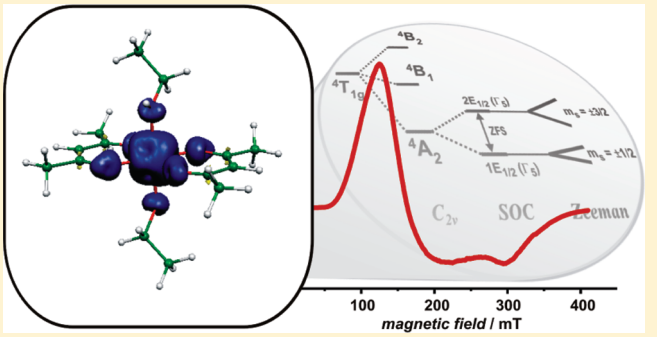

1. INTRODUCTION

Bis-2,4-pentanedionato(acetylacetonate)cobalt(II), $Co(acac)_2$, is one of the typical synthons used in the coordination chemistry of cobalt.[1−4] Recently, much attention has been paid to common and easily available $Co(acac)_2$ complexes and their fluorinated derivatives, which were found to mediate radical polymerization of polar monomers, such as vinyl acetate, in the controlled radical polymerization (CRP) processes.[5−7] The CRP mechanism is based on the concept of radical concentration decrease in the reaction medium by reversible conversion of growing macroradicals to dormant species, lowering the probability of irreversible termination.[8] It can be accomplished either by a thermodynamically neutral bimolecular exchange between propagating radicals and a dormant species or by a spontaneous reversible homolytic cleavage of the dormant chain end, depending on the absence/presence of electron-donor ligands in the polymerization environment.[7] However, thorough examination of the mechanism of the $Co(acac)_2$-mediated polymerization is still a challenging issue, i.a., due to the difficulties in determination of the lowest-energy spin state and preferred geometry of the key $Co(acac)_2$ complex under the reaction conditions.[9]

One of the characteristic features of divalent cobalt implicated by its $3d^7$ electronic configuration is the presence of two spin states, a doublet $^2Co^{II}$ ($S = 1/2$) and a quartet $^4Co^{II}$ ($S = 3/2$) one, depending on the chemical environment. In principle, they can be distinguished with the help of electron paramagnetic resonance (EPR) spectroscopy. Transitions between those two states lead to spin crossover, which is an important factor affecting both the thermodynamics and kinetics of the ligation processes, giving rise to two-state reactivity of cobalt(II) complexes.[10,11]

In the case of a monomeric $Co(acac)_2$ complex, not only two alternative spin states but also two different conformations (square-planar or tetrahedral) should be considered. Several possible structures have been identified in the solid state, including polynuclear (tetrameric)[1,2] and anhydrous monomeric $Co(acac)_2$ complexes.[3,12] For noncoordinating solvents, on the basis of molecular weight measurements as well as from visible and near-IR spectroscopy, the $Co(acac)_2$ complex was found to assume a mononuclear tetrahedral structure in dilute solutions and octahedral oligomeric structure at higher concentrations.[4] Magnetic measurements of the solid $Co(acac)_2$ imply a high-spin state of cobalt, which is supposed to be preserved also in noncomplexing solvents.[13] This issue, however, has not been resolved definitely as yet. According to the available data, solutions of the $Co(acac)_2$ complexes in toluene were described as EPR-silent,[9] most probably because the temperature of those measurements was not sufficiently low for detecting fast relaxing Co(II) species.

Due to possible existence of low-spin (LS) and high-spin (HS) states, Co(II) complexes are also a challenging subject for computational chemistry.[14] Already, the crystal-field theory is able to disclose the nature of the difficulties. Considering the common octahedral geometry, the low-spin state (^2E_g) of Co(II)

Received: October 4, 2010
Revised: February 1, 2011
Published: February 25, 2011

complexes corresponds to the electronic configuration $(t_{2g})^6(e_g)^1$, whereas the high-spin state ($^4T_{1g}$) corresponds to $(t_{2g})^5(e_g)^2$ in an idealized octahedral notation. For simplicity, the Jahn−Teller effect has been ignored although both states are orbitally degenerate. For such states, the electronic energy difference $E_{HS} - E_{LS}$ is given by $12Dq - 7B - 4C$,[15] where $10Dq$ is the crystal-field splitting parameter and B and C are the Racah parameters of the interelectronic repulsion for the same maximum spin multiplicity, and different spin multiplicities, respectively. It becomes thus evident that a large crystal-field splitting favors the LS state, whereas strong interelectronic repulsion and a weak ligand field favor the HS state. As a consequence, any theoretical method that aims at quantitative prediction of the $E_{HS} - E_{LS}$ energy gap must be well-balanced in order to correctly predict the interplay between $10Dq$ (being dominated by metal−ligand bonding) and interelectronic repulsion (being dominated by dynamic correlation effects within the d-shell).

As expected, the Hartree−Fock (HF) method is strongly biased in favor of HS states as it neglects electron correlation. On the other hand, the standard density functional theory (DFT) methods with "pure" XC functionals, widely applied to describe transition metal complexes,[16,17] have an opposite bias in favor of the LS states and exhibit rather poor performance in the case of relative energy calculations for the states with different spin multiplicity.[18] Hybrid functionals, being better balanced, are essentially superior than the HF or "pure" DFT methods;[19−21] however, a "universal" hybrid functional dedicated to the spin-state problems is not available yet.[22]

As the main goals, the present study includes (1) probing the ground spin state of $Co(acac)_2$-based complexes by EPR spectroscopy at liquid helium temperature, (2) determination of the LS and the HS structures of the parent $Co(acac)_2$ and derivative $Co(acac)_2L_n$ complexes with water and ethanol coligands by geometry optimization using both gradient-corrected and hybrid exchange-correlation functionals, and (3) calculation of spin-Hamiltonian parameters (electronic **g** tensor, hyperfine **A** tensor, and zero-field splitting parameters) by relativistic DFT techniques.

2. EXPERIMENTAL METHODS

The $Co(acac)_2$ sample was synthesized in a reaction of $Co(NO_3)_2 \cdot 6H_2O$ (1 g), dissolved in 40 mL of water, with 5 mL of 2,4-pentanedione. While stirring, a small amount of solid Na_2CO_3 was added until pink platelike crystals precipitated from the solution. The resultant solid was filtered, washed, and next refluxed in ethanol for 1 h. The reaction mixture was left to cool down, and the final product was separated.

X-band EPR spectra were recorded with a Bruker ELEXSYS-500 spectrometer using a rectangular TE_{102} cavity and 100 kHz modulation. Variable temperature measurements were carried out with a liquid helium ESR900 cryostat (Oxford Instruments) in the temperature range of 5−300 K. For the EPR measurements, a 1 mM solution of $Co(acac)_2$ in toluene/ethanol glass (7:3 vol) was used. Electronic absorption spectra were recorded with a Shimadzu UV-3600 spectrophotometer.

3. COMPUTATIONAL DETAILS

DFT calculations for $Co(acac)_2$ structures were performed with the Amsterdam density functional (ADF) program (versions 2004.01 and 2007.01).[23−27] Geometry optimization was based on the gradient-corrected Becke−Perdew (BP)[28−30] and Becke−Lee−Yang−Parr (BLYP)[28,31] exchange-correlation functionals. A standard double-ζ STO basis with one set of the polarization functions (DZP) was used for main-group elements (H, C, O), whereas a standard triple-ζ basis set (TZP) was employed for cobalt. The 1s electrons of C and O, as well as the 1s−2p electrons of Co, were treated as frozen cores. Auxiliary *s*, *p*, *d*, *f*, and *g* STO functions, centered on all nuclei, were used to fit the electron density and to obtain an accurate Coulomb potential in each SCF cycle. Relativistic effects were included using the first-order scalar relativistic correction.[32−34] Optimized geometries were further used in a full-electron single-point energy calculations in order to evaluate their energies with both gradient-corrected (BP and BLYP) and hybrid functionals (B3LYP with 20% of the Hartree−Fock exchange[35,36] and its modified form B3LYP* with 15% of the Hartree−Fock exchange[19]).

To account for direct electron exchange effects, for the complexes with additional ligands $Co(acac)_2L_n$ (where L = H_2O, EtOH, n = 1 and 2) optimization of the geometry was performed with the Gaussian03 program (version E.01).[37] The hybrid B3LYP exchange-correlation functional and all-electron Ahlrichs triple-ζ type (TZV)[38] basis set with one set of the polarization functions were used.

The optimized structures were next applied for spectroscopic calculations. Calculations of the electronic **g**, hyperfine **A**, and the zero-field splitting **D** tensors were performed with the ORCA package.[39] In the case of zero-field splitting (ZFS) direct spin−spin (SS) and spin−orbit couplings (SOC), calculated according to Neese,[40] were taken into account. BP and B3LYP exchange-correlation functionals were applied along with the TZV(P)[38] basis set for the ligands and TZV(PPP)[38] for cobalt. For the estimation of the SOC effects (for **g**, **A**, and ZFS) the mean-field approximation (SOMF), including both the spin-own-orbit and spin-other-orbit interactions in the exchange term as well as coupled-perturbed approach (CP), was carried out. The SS contributions were included on the basis of the spin-density formula.[41]

4. RESULTS AND DISCUSSION

4.1. DFT Calculations for $Co(acac)_2$ Monomer. The optimized geometries of the square-planar and tetrahedral conformations of the $Co(acac)_2$ complex obtained with the BP functional are shown in Figure 1, where the Co−O distances and the O−Co−O angles derived from BP and BLYP calculations are also reported. The relative energies for all investigated species and calculations with different functionals are collected in Table 1.[42]

Inspection of the geometrical parameters of the $Co(acac)_2$ complex optimized with the BP functional in both spin states showed that the Co−O bond length increases significantly for the high-spin structures, from 1.85 Å for the square-planar doublet to 1.94 and 1.96 Å for the tetrahedral and square-planar quartets, respectively. Each of the optimized structures differs also in the size of the O−Co−O angle. It decreases in the following order: tetrahedral quartet (97.7°) > square-planar doublet (95.0°) > square-planar quartet (90.5°). The optimized Co−O distances for the high-spin $Co(acac)_2$ complexes are close to the experimental values, determined for tetrameric tetrahedral (1.93−2.13 Å)[2] and monomeric square-planar (1.92 Å) anhydrous $Co(acac)_2$ complexes.[3] In the latter case, the experimental value of the O−Co−O angle (93.4°) is situated between the

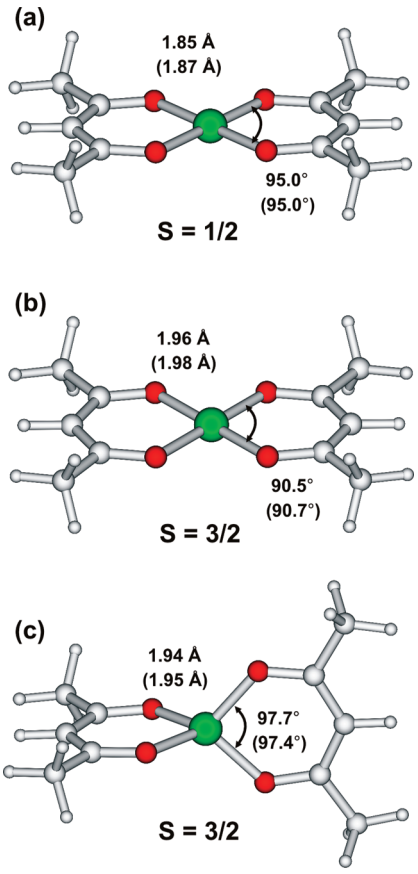

Figure 1. DFT-optimized geometries of the square-planar $Co(acac)_2$ complex in (a) doublet and (b) quartet spin states, and (c) the tetrahedral structure in quartet spin state using BP exchange-correlation potential. The numbers in parentheses correspond to the structures optimized with BLYP XC functional.

Table 1. Relative Energies for Different Structures of the $Co(acac)_2$ Complexes

		ΔE/kcal·mol^{-1}			
		GGA functionals		hybrid functionals	
geometry	S	BP	BLYP	B3LYP	B3LYP*
square-planar	1/2	0.00[a]	0.00[b]	10.18[a]	5.72[a]
				10.11[b]	5.66[b]
tetrahedral	3/2	4.89[a]	4.84[b]	0.00[a]	0.00[a]
				0.00[b]	0.00[b]
square-planar	3/2	15.90[a]	14.80[b]	9.48[a]	9.75[a]
				9.43[b]	9.67[b]

[a] Geometry optimized with the BP XC functional. [b] Geometry optimized with the BLYP XC functional.

values calculated for the square-planar spin doublet and the spin quartet.[3]

The change of the XC functional did not lead to a significant alternation of the complex geometry. The structural parameters shown in Figure 1 demonstrate that, indeed, the BP and BLYP geometries differ only slightly. Changes in the Co−O bond length remain within the range of 0.01−0.02 Å, and differences in the O−Co−O angle are of the order of 0.1−0.2°. Comparison of

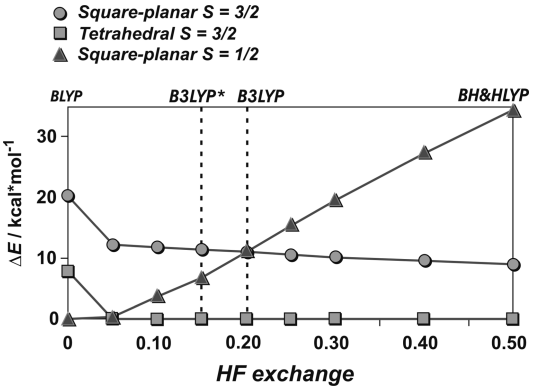

Figure 2. Relative energies of the electron spin states of the $Co(acac)_2$ complex in square-planar (S = 1/2 and 3/2) and tetrahedral (S = 3/2) conformations obtained with increasing admixture of exact (Hartree−Fock) exchange to the BLYP exchange-correlation functional.

the BP and BLYP geometries of the quartet tetrahedral structure with the corresponding B3LYP results by Maria et al.[7] shows again that use of the hybrid functional has a small influence on the geometry. The corresponding values of the Co−O distance and the O−Co−O angle were found to be 1.95 Å and 95.8°, respectively.

The energy differences obtained for the gradient-corrected BP and BLYP functionals are collected in Table 1. Both functionals predict a doublet spin ground state in the square-planar geometry of the investigated complex. The quartet spin state of the tetrahedral geometry is higher in energy by 4.9 and 4.8 kcal/mol for BP and BLYP, respectively. The energy of the square-planar quartet structure, in turn, is higher by 15.9 kcal/mol for BP and 14.8 kcal/mol for BLYP. Thus, it may be concluded that both gradient-corrected functionals lead to similar predictions, with the low-spin state in the square-planar geometry as a possible ground state of the isolated $Co(acac)_2$ complex.

However, the more involved hybrid functionals led to opposite results. The ΔE values collected in the last two columns of Table 1 show that the tetrahedral quartet has the lowest energy for B3LYP and B3LYP*. The energies of the square-planar structure in the quartet spin state are comparable for both functionals, but are higher by 9.4−9.8 kcal/mol with respect to the tetrahedral structure. The energy of the low-spin state of the $Co(acac)_2$ complex is higher than that of the high-spin ground state by 10.2 and 5.7 kcal/mol for B3LYP and B3LYP*, respectively. It should be pointed out that the choice of the geometry (obtained with BP or BLYP) has a negligible effect on the relative energies presented in Table 1.

The differences obtained for both gradient-corrected and hybrid functionals show that the energetic preference of the high-spin state with respect to the low-spin state increases with the enhanced fraction of the exact (Hartree−Fock) exchange. The change in the spin ground state is especially apparent when comparing relative energies of the involved conformations, calculated according to the adiabatic equation[35] $E_{xc} = aE_x^{B88} + (1 - b)E_x^{LSDA} + bE_x^{HF} + cE_c^{LYP} + (1 - c)E_c^{VWN}$ with increasing exact HF exchange E_x^{HF} (parameter b) in the modified B3LYP functional (Figure 2). For the gradient-corrected functional (with b = 0%) the low-spin state is preferred. For small admixture of the HF exchange (b = 5%), the doublet and quartet states are almost degenerate, whereas upon passing from b = 10% to B3LYP* (b = 15%) and B3LYP (b = 20%) the doublet state is

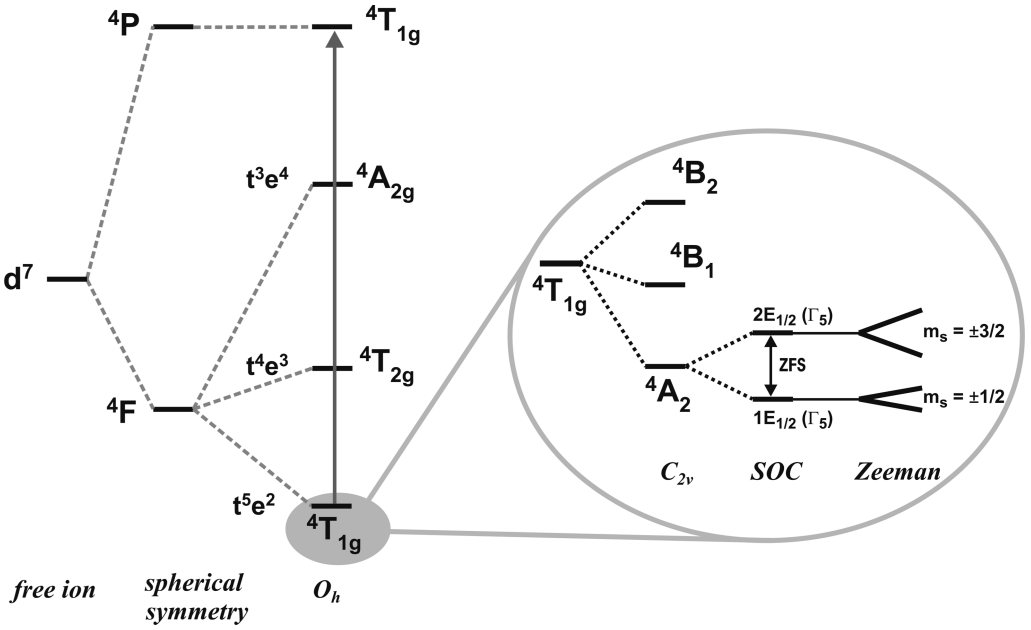

Figure 3. Crystal-field diagram of energy levels under spin−orbit and Zeeman interactions for six-coordinate high-spin cobalt(II) complexes. An arrow indicates the main transition observed in optical absorption spectrum.

increasingly destabilized by 4, 6, and 10 kcal/mol, respectively. The results are in line with the findings obtained by Reiher et al.[19] who showed that for correct prediction of LS−HS energy gap at least 8% of E_x^{HF} is necessary.

The B3LYP energy difference between the square-planar doublet and the tetrahedral quartet obtained by us (10.2 kcal/mol) is in line with the corresponding value calculated previously (8.8 kcal/mol).[7] Most likely such a difference can be attributed to the discrepancies between both calculation schemes.

In conclusion, it was demonstrated here that "pure" DFT functionals predict the square-planar doublet as the ground state of the $Co(acac)_2$ complex, whereas hybrid functionals distinctly favor the tetrahedral quartet structure. For such cases, application of high-level ab initio electron correlation methods[14] or experimental determination of the ground state[13] of the investigated complex is required, in order to validate the choice of the XC functional. In a very recent X-ray diffraction (XRD) study,[12] however, a monomeric $Co(acac)_2$ complex has been found in the tetrahedral conformation, supporting the choice of the hybrid functional for DFT calculations, in agreement with EPR arguments (vide infra).

4.2. EPR Measurements. The ambiguity of high-spin versus low-spin ground state of the $Co(acac)_2$ complex with respect to the selection of an adequate exchange-correlation functional can be resolved with the aid of the EPR spectroscopy.[43] The $3d^7$ electronic configuration of Co^{2+} implies a ^4F ground state for the free ion. A simplified energy level diagram of the high-spin cobalt(II) based on crystal-field and symmetry considerations showing influence of a rhombic distortion (C_{2v}) and SOC is presented in Figure 3. The cubic ligand field and the SOC effects give rise to an orbitally nondegenerate $^4A_2$ or an orbitally degenerated $^4T_1$ states (derived from octahedral coordination), depending on the actual ligand arrangement.[44,45] The combined action of the symmetry distortion and the SOC leads to the splitting of two Kramers doublets ($m_s = \pm 1/2$ and $m_s = \pm 3/2$). This effect is known as the zero-field splitting and is gauged by $|\Delta| = 2(D^2 + 3E^2)^{1/2}$ value, where D and E are the axial and rhombic ZFS parameters, respectively. The $^4A_2$ ground state with the quenched orbital momentum is typical for tetra- or penta-coordinate cobalt(II). Neglecting the rhombic deformation, the sign of Δ value determines whether or not the $m_s = \pm 1/2$ or $m_s = \pm 3/2$ state is the lowest. In the presence of magnetic field **B**, two degenerate spin doublets are split, and the incident microwave radiation will induce transitions according to the selection rule $\Delta m_s = \pm 1$. For positive values of Δ, when $|\Delta| \gg h\nu$, the $m_s = \pm 1/2$ or $m_s = \pm 3/2$ states become well-separated, and the Co(II) paramagnet can be described by an effective spin $S_{eff} = 1/2$. However, the low-lying excited level $m_s = \pm 3/2$ leads to fast relaxation; therefore, such spectra can be observed exclusively at liquid helium temperatures, allowing for simple distinction between the high- and low-spin states of the investigated complex.

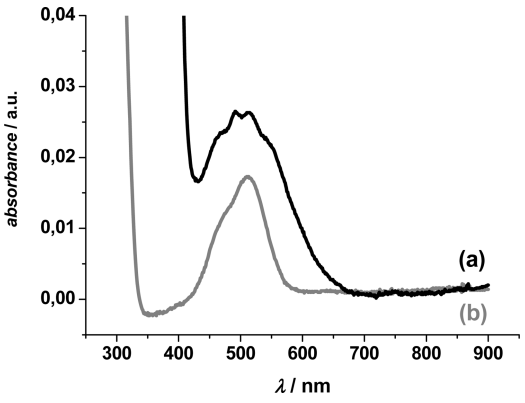

Figure 4. Electronic absorption spectra of (a) $Co(acac)_2$ in toluene/ethanol (7:3) solution and (b) $Co(NO_3)_2$ in H_2O.

A low-spin $S = 1/2$ state is likely to occur when Co^{2+} ions are in a square-planar or square-pyramidal environment such as $\{CoN_4\}$ or $\{CoN_2O_2\}$.[43] Two possible ground states, $^2A_2$ or $^2A_1$, associated with d_{yz} and d_{z^2} semioccupied molecular orbitals (SOMO), respectively, can be distinguished based on the

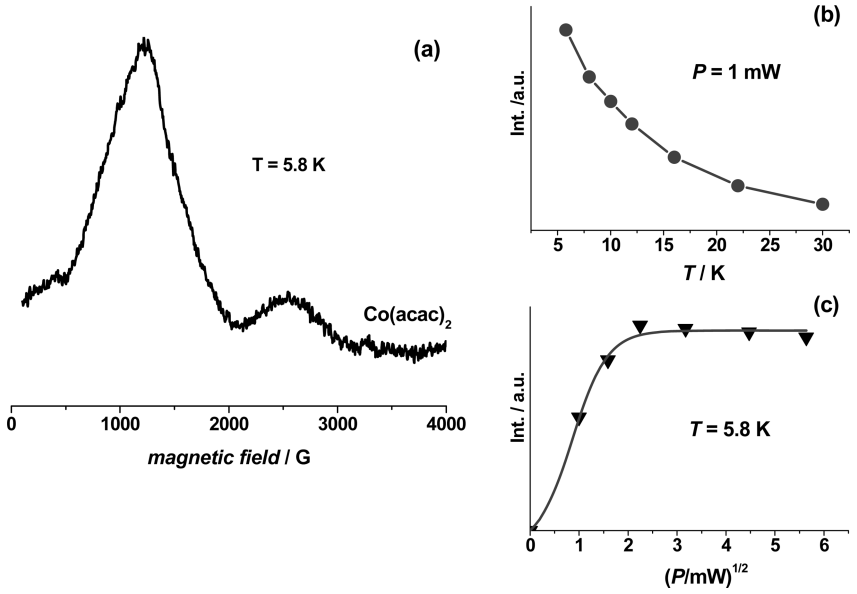

Figure 5. (a) X-band EPR spectrum of the $Co(acac)_2$ complex measured in a toluene/ethanol (7:3) glass at 5.8 K along with (b) temperature dependence of the EPR signal intensity for the $Co(acac)_2$ complex, measured in the temperature range from 5 to 30 K at microwave power of $P = 1$ mW, and (c) the saturation profile obtained at 5.8 K.

analysis of the **g** and **A** tensor anisotropies. The values of $g_z \sim 2.0 < g_{x,y}$ and $A_z > A_{x,y}$ are indicative for the $^2A_1$ state, whereas the opposite ordering is valid for the $^2A_2$ ground state.[46] Owing to the usually well-separated energy levels, the EPR spectra of the low-spin Co(II) can be observed already at liquid nitrogen temperature and are characterized by an anisotropy smaller than that characteristic of the $S = 3/2$ species.

For the EPR measurements, $Co(acac)_2$ solid was dissolved in a toluene/ethanol solution. Since $Co(acac)_2$ is known for its ability of coordinating molecules of polar solvents,[7,13] it is likely that the actual composition of the examined complex is either $Co(acac)_2(EtOH)_2$ (EtOH = ethanol) or $Co(acac)_2(H_2O)_2$ (due to water present in ethanol). By comparing the electronic UV−vis absorption spectrum of the obtained solution (Figure 4a) with that containing cobalt(II) nitrate in water (Figure 4b), indeed an expansion of the coordination sphere of cobalt(II) upon dissolution, from the tetrahedral to the octahedral one, can be deduced. The UV−vis signal of the latter is characteristic of a hexacoordinated $Co(H_2O)_6^{2+}$ cation. The spectrum is centered at 515 nm due to the $^4T_{1g}(F) \rightarrow {}^4T_{1g}(P)$ transition (Figure 3) with a shoulder at 470 nm resulting from the SOC in the excited $^4T_{1g}(P)$ state that lifts its degeneracy. Additionally, a slight splitting of the bands is associated with lowering of the local O_h symmetry in the $Co(acac)_2(EtOH)_2$ complex to C_{2v} (Figure 3), which is close to the actual geometry derived from the DFT calculations (see section 4.3).

The X-band EPR spectrum of the $Co(acac)_2$ complex recorded at 5.8 K in a toluene/ethanol glass is shown in Figure 5a. The spectrum is dominated by two broad features with apparent $g_\perp \approx 5.8-5.4$ and $g_{||} \approx 2.0$, due to the resonances occurring when the magnetic field is coincident with the perpendicular (stronger feature) and parallel (weaker feature) directions of the complex. The effective *g*-values are in line with those of other molecular complexes of cobalt(II) with oxygen-donor ligands.[43] There is no evidence of even poorly resolved hyperfine structure due to the ^{59}Co ($I = 7/2$, 100%) nucleus, in contrast to low-spin complexes, where a hyperfine pattern is often observed. The EPR signal was detectable only below 40 K, implying a clear high-spin quartet state of the $Co(acac)_2$ complex. Then the observed spectrum can be rationalized in terms of an axial spin-Hamiltonian $\hat{H}_s = \mu_B \mathbf{B}\hat{\mathbf{g}}\vec{\mathbf{S}} + D[\vec{\mathbf{S}}_z^2 - S(S+1)/3]$ with $S = 3/2$. However, due to the large width of the EPR signal spanning 350 mT, accurate spin-Hamiltonian parameters cannot be extracted from such a powder spectrum registered at X-band only.

The sign of Δ parameter can be determined from the temperature-dependent measurements. It is positive when $m_s = \pm 1/2$ is the ground state and gives rise to Curie−Weiss behavior, whereas negative value of Δ, consistent with the $m_s = \pm 3/2$ ground state, results in a non-Curie−Weiss attitude. Figure 5b shows the intensity of the EPR signal of the $Co(acac)_2$ frozen solution measured as a function of temperature in the range of 5−30 K. The microwave power saturation curve (Figure 5c) shows that the saturation of the high-spin $Co(acac)_2$ signal occurs above 3 mW at 5.8 K. The obtained results indicate a clear Curie−Weiss behavior for the examined complex with the $m_s = \pm 1/2$ doublet being lower in energy. Since the resonance transitions were observed only within the $m_s = \pm 1/2$ Kramers doublet, the ZFS value fulfills the condition $\Delta \gg h\nu$. In such a case, the effective *g*-factors are equal to $g_{\text{eff},\perp} \sim 4 \div 5$ and $g_{\text{eff},||} \sim 2$,[47] in accordance with the experiment. Assuming that the spin relaxation is dominated by the Orbach process ($1/T_1 \sim \Delta^3 \exp(-\Delta/kT)$),[48] the close-lying $m_s = \pm 3/2$ state (separated by the ZFS parameter Δ) accounts for fast relaxation, leading to a very broad EPR signal of the high-spin $Co(acac)_2(EtOH)_2$ complex even at liquid helium temperatures, as was actually observed.

The observed EPR features of the $Co(acac)_2(EtOH)_2$ complex are thus diagnostic of the high-spin state of the Co(II) core. There is an axial distortion of the complex leading to $\Delta \gg h\nu$, but evidently not strong enough to impose a low-spin configuration.

4.3. DFT Calculations for $Co(acac)_2L_n$ Complexes. On the basis of the above results, DFT modeling for the $Co(acac)_2L_n$ (L = EtOH, H_2O) complexes was carried out with hybrid exchange-correlation functional in the B3LYP parametrization.

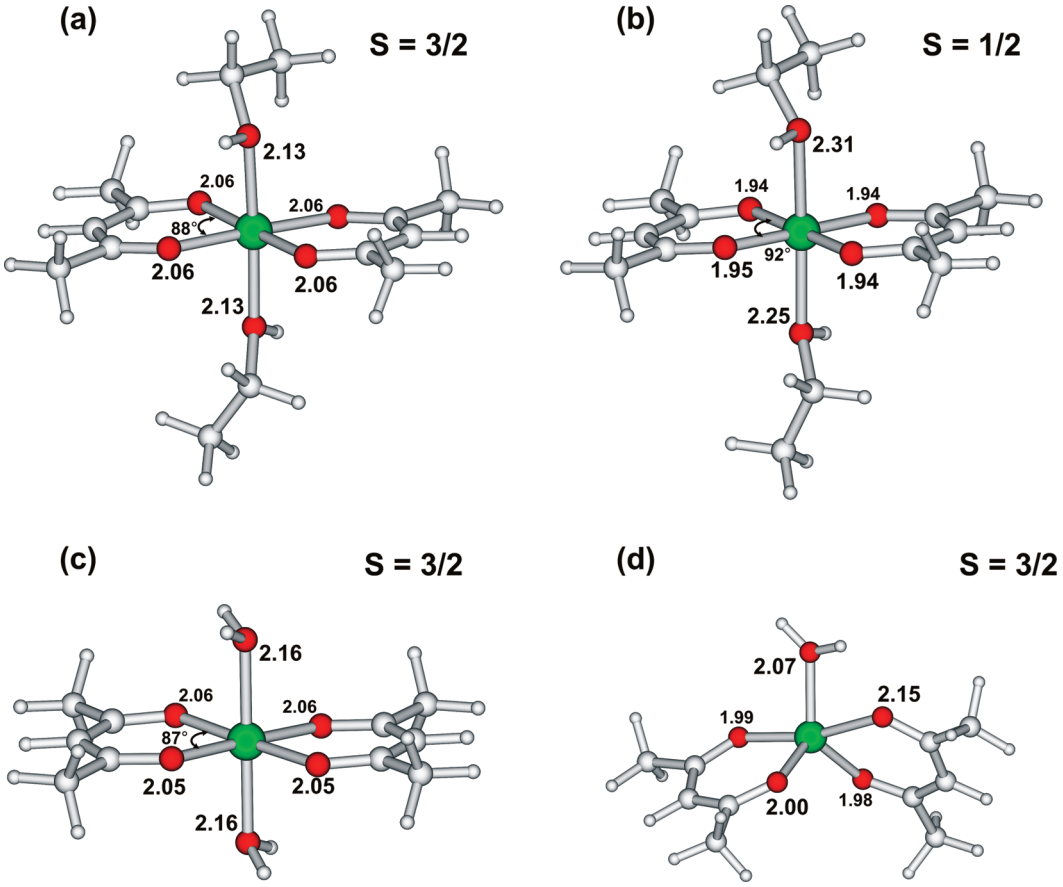

Figure 6. Optimized geometries (B3LYP/TZV) of the $Co(acac)_2(EtOH)_2$ complex in (a) the quartet and (b) the doublet spin states along with (c) diaqua $Co(acac)_2(H_2O)_2$ and (d) monoaqua $Co(acac)_2(H_2O)$ structures in the quartet spin state. All bond lengths are given in angstroms, and angles are given in degrees.

Table 2. Relative Energies for the Structures of the $Co(acac)_2(H_2O)_n$ (n = 1, 2) and $Co(acac)_2(EtOH)_2$ Complexes Obtained with the B3LYP Functional

	ΔE/kcal·mol^{-1}	
structure	S = 1/2	S = 3/2
$Co(acac)_2(H_2O)$	16.86	0.00
$Co(acac)_2(H_2O)_2$	14.50	0.00
$Co(acac)_2(EtOH)_2$	8.09	0.00

The resultant structures of $Co(acac)_2(EtOH)_2$, $Co(acac)_2(H_2O)_2$, and $Co(acac)_2H_2O$ are shown in Figure 6, where the Co−O distances and the O−Co−O angles are also reported. The relative energies for the low- and high-spin states are collected in Table 2.

Unlike for the four-coordinated complexes, the six-coordinated ones exhibit no ability for planar−cubic geometry transformation. Thus, the structures of $Co(acac)_2(EtOH)_2$ optimized with the B3LYP functional in both spin states are found generally to be quite similar. As in preliminary calculations, Co−O bond length increases significantly for the high-spin structure, from 1.94 Å for the doublet (Figure 6b) to 2.06 Å for the quartet geometry (Figure 6a), but only for the acac ligands. The opposite trend is observed for the coordinated ethanol. The Co−OH bond lengths for the LS state (2.31 Å and 2.25 Å) decrease sharply to its characteristic average value of 2.16 Å when passing to the HS state. As a result, the HS quartet state gains in bonding energy and becomes the ground state of the complex (8.09 kcal/mol below the doublet). The optimized HS geometry was found to be very similar to the crystal structure determined from XRD measurements.[12] A slight difference consists of the XRD Co−OH bond length equal to 2.186 Å as compared to 2.130 Å obtained from DFT optimization.

The structure of $Co(acac)_2(H_2O)_2$ in the high-spin state (Figure 6c) is very similar to the high-spin structure of $Co(acac)_2(EtOH)_2$. The Co−O bond lengths are found in a range of 2.05−2.06 Å, whereas two H_2O molecules are placed at the equal distance of 2.16 Å. Thus, the nearest chemical environments of the $Co(acac)_2(H_2O)_2$ and $Co(acac)_2(EtOH)_2$ complexes form a polyhedron with the approximate C_{2v} point symmetry (this was assumed also in Figure 3).

The monoaqua complex $Co(acac)_2H_2O$ in the quartet state, shown in Figure 6d, exhibits an irregular five-coordinated structure with unequal cobalt−acac bond lengths. For all considered $Co(acac)_2L_n$ structures, the Co−OH_2 distance (2.07 Å) is the shortest among the Co−L bonds. It is formed at the expense of one of the bonds formed with the acac ligand, which is found to be as long as 2.15 Å. Two six-membered rings of the $Co(acac)_2$ unit are twisted by 56° with respect to each other, whereas for all other structures the rings are approximately coplanar.

The energy differences of the HS and LS states obtained with the hybrid B3LYP functional are collected in Table 2. In analogy

Table 3. DFT-Calculated Spin-Hamiltonian Parameters (Zero-Field Splitting D and E, g Tensor, and Hyperfine ^{Co}A Tensor) for the $Co(acac)_2(H_2O)_n$ (n = 0, 1, 2) and $Co(acac)_2(EtOH)_2$ Complexes

	ZFS		g tensor			^{Co}A tensor/MHz		
structure	D/cm^{-1}	E/D	g_{11}	g_{22}	g_{33}	A_{11}	A_{22}	A_{33}
$Co(acac)_2$ tetrahedral	−31.42	0.058	2.076	2.078	2.119	−82	−90	−91
$Co(acac)_2$ square-planar	39.98	0.133	2.047	2.150	2.158	4	−41	−229
$Co(acac)_2(H_2O)$	−5.06	0.211	2.091	2.100	2.114	−17	−82	−119
$Co(acac)_2(H_2O)_2$	43.46	0.058	2.070	2.111	2.135	−4	−68	−142
$Co(acac)_2(EtOH)_2$	16.56	0.086	2.081	2.098	2.155	−25	−85	−107

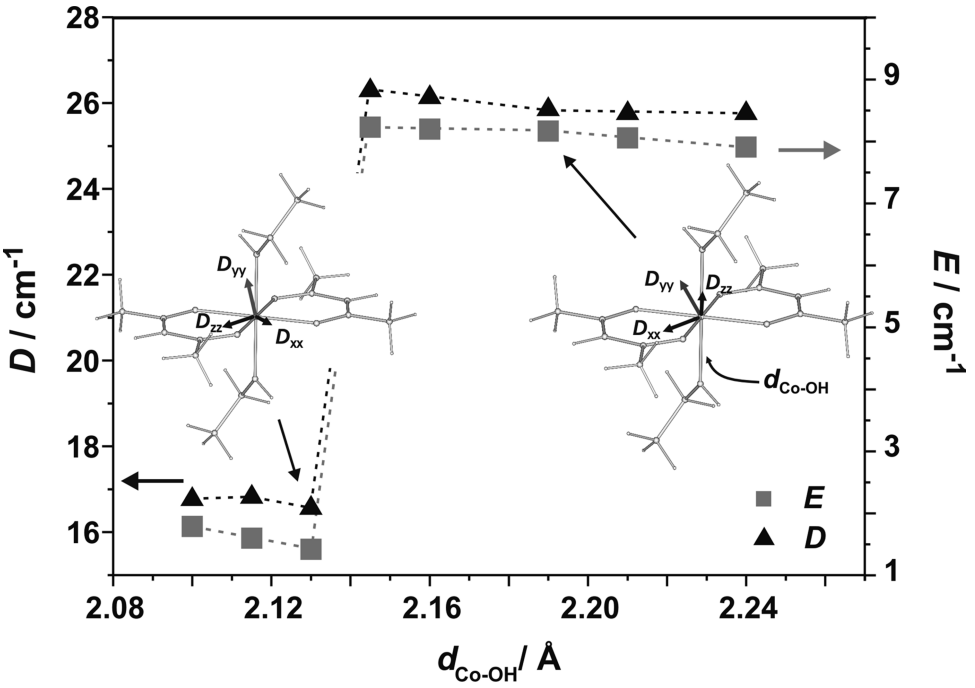

Figure 7. Calculated changes in D and E parameters for the $Co(acac)_2(EtOH)_2$ complex with respect to the elongation of the Co−OH bond along with the orientation of the **D** tensor axes shown for two d_{Co-OH} values characteristic of DFT optimization (2.130 Å) and crystallographic structure (2.186 Å).

to the $Co(acac)_2$ structure, calculations have predicted a quartet spin ground state for all $Co(acac)_2L_n$ complexes. The energy differences are of similar magnitude as for $Co(acac)_2$ with the highest value obtained for the five-coordinated monoaqua complex. As a result, regardless of the coordination number, all $Co(acac)L_n$ complexes, with L = EtOH or H_2O, exhibit quartet spin state with $S = 3/2$, in agreement with the EPR findings.

4.4. Calculation of Spin-Hamiltonian Parameters. In case of unresolved zero-field features in the EPR spectrum of the $Co(acac)_2(EtOH)_2$ complex (Figure 5a) DFT calculations of the spin-Hamiltonian parameters may help to recover the lost information. The obtained **D**, **g**, and **A** parameters for the investigated complexes are listed in Table 3. On the basis of the D and E values, the calculated splitting of the $m_s = \pm 1/2$ and $m_s = \pm 3/2$ states gauged by the $|\Delta| = 2(D^2 + 3E^2)^{1/2}$ value varies between 10 and 87 cm^{-1}. Bearing in mind that the EPR spectra were recorded in X-band (with microwave energy of ca. 0.3 cm^{-1}), it becomes obvious that the observed transitions occur within the lowest $m_s = \pm 1/2$ state only (see Figure 3). Thus, all the investigated $Co(acac)_2L_n$ complexes behave as effective $S_{eff} = 1/2$ doublet systems. Consequently, the g-values extracted from the spectrum represent effective values ($g_\perp \approx 5.8-5.4$ and $g_{||} \approx 2.0$) and do not provide adequate discrimination between the four, five, or six coordination.[49] The actual **g** tensor components calculated with the B3LYP-SOMF method are shown in Table 3. In the case of cobalt hyperfine splitting, the calculated maximal component of the **A** tensor for $Co(acac)_2(EtOH)_2$ corresponds to 42 G. Thus, the particularly large line widths of 500 G observed in the EPR spectrum (Figure 5a) suppress direct measurement of cobalt **A** tensor parameters either. Taking into account the calculated spin-Hamiltonian parameters, the EPR spectrum with resolved features could only be obtained with a high-frequency, high-field EPR technique (HF-EPR)[50] with microwave frequency of at least 1000 GHz (energy limit based on the Δ value calculated for $Co(acac)_2(EtOH)_2$).

As has been pointed out on the basis of experimental[45,51] and theoretical studies,[52] the ZFS parameters are very sensitive to the molecular geometry of $S > 1/2$ systems. In the case of the investigated Co(II) complexes, the results obtained with DFT methods (Table 3) clearly show the differences of ZFS parameters originating from the structural changes around the cobalt center. The most discriminating factor is the arrangement of two acac ligands. In the case when both ligands are twisted, such as for

Table 4. Individual Contributions to the Zero-Field Splitting D and E Parameters for the $Co(acac)_2(EtOH)_2$ Complex, Computed with the CP-DFT Method (B3LYP/TZVPP) and the SOMF Operator

contribution	D/cm^{-1}	E/cm^{-1}
1. α → α (SOMO → VMO)	9.91	−0.05
2. β → β (DOMO → SOMO)	14.18	−2.03
3. α → β (SOMO → SOMO)	−6.36	2.64
4. β → α (DOMO → VMO)	−0.75	−0.04
spin−orbit (1 + 2 + 3 + 4)	16.98	0.53
spin−spin	−0.42	0.90
total	16.56	1.43

tetrahedral $Co(acac)_2$ and five-coordinated $Co(acac)_2(H_2O)$ complexes, the calculated D parameter was found to be negative. On the other hand, for coplanar acac ligands the D parameter was positive, as can be observed for square-planar $Co(acac)_2$ and six-coordinated $Co(acac)_2(H_2O)_2$ and $Co(acac)_2(EtOH)_2$ structures.

The calculated orientation of principal components of the zero-field splitting tensor **D** with respect to the molecular framework of the $Co(acac)_2(EtOH)_2$ complex is shown in Figure 7. The calculated values of the principal components are equal to $D_{xx} = -4.10\ cm^{-1}$, $D_{yy} = -6.94\ cm^{-1}$, and $D_{zz} = 11.04\ cm^{-1}$. The D_{xx} and D_{zz} axes are approximately located in the plane of acac ligands, bisecting the angles between Co−O bonds. The D_{yy} axis, tilted about 20° outward of the Co−EtOH bond, points toward the OH group of the coordinated ethanol molecule (Figure 7, left-hand side structure). Because of the well-known sensitivity of the ZFS parameters to the geometrical parameters (see Table 3), taking into account an appreciable underestimation of the calculated Co−EtOH bond length as compared to the crystallographic distance,[12] we performed additional CP-B3LYP-SOMF calculations to evaluate the response of the D and E values to the changes in d_{Co-OH} distance. The results, depicted in Figure 7, indicate two stable regions with D values of around 17 and 26 cm^{-1}, delineated by a critical distance of $d_{Co-OH} \approx 2.13$ Å. The calculations revealed also that the sudden increase of both D and E values is accompanied by the change in the orientation of the principal **D** tensor axes, with the direction of the biggest D_{zz} component being twisted from the acac plane toward the ethanol ligand, as the d_{Co-OH} distance is increased above the critical value (Figure 7). Thus, for the experimental d_{Co-OH} values (derived, e.g., from XRD measurements), the expected ZFS parameter is around $D = 26\ cm^{-1}$ ($\Delta \approx 60\ cm^{-1}$, in line with EPR data for similar systems[45]), whereas for the calculated d_{Co-OH} values D parameter is around 16−17 cm^{-1} only, apparently due to underestimation of the Co−OH distance.

More insight into the electronic nature of the ZFS parameters can be obtained upon partitioning of the zero-field effect into the first- and the second-order contributions. Such partition was performed for the experimentally observed $Co(acac)_2(EtOH)_2$ complex (section 4.2). The results obtained with the B3LYP-CP-SOMF technique are shown in Table 4. They indicate that the dominant contribution to the total D value originates from the second-order SOC with the magnitude of $D_{SOC} = 16.98\ cm^{-1}$. The first-order SS interaction amounts to $D_{SS} = -0.42\ cm^{-1}$ only. Similar results have been obtained for other tetrahedral cobalt(II) complexes.[52] The dominant SOC part can be further factorized into four types of excitations. The first one, coupling between the semioccupied (SOMO) and the virtual molecular orbitals (VMO), leads to single determinants of the same total spin as the ground state ($S' = S$) and occurs between the spin-up electrons (α → α). The second one, between the doubly occupied (DOMO) and SOMO orbitals, is also a spin-allowed transition ($S' = S$) but involves spin-down states (β → β). The third one, SOMO(α) → SOMO(β), leads to single determinants, with the total spin $S' = S - 1$, and represents the so-called spin-flip excitations.[53] For the last transition, DOMO(β) → VMO(α), the spin of the excited electron is flipped such a way that the total spin is $S' = S + 1$. For the investigated complex, the α → α and β → β excitations makes the largest contributions to D_{SOC}, which is further modified mostly by the α → β (quartet → doublet) spin-flip excitation. Because the dominant magnetic couplings greatly involve the SOMO state, the ZFS parameters are very sensitive to the local surrounding of high-spin cobalt(II), as shown in Table 3.

5. CONCLUSIONS

The DFT-optimized geometries of the $Co(acac)_2$ complex were found to be critically spin-state sensitive, showing that in the case of "pure" DFT functionals a square-planar conformation is associated with the spin doublet, whereas for the spin quartet a tetrahedral conformation is preferred. Hybrid B3LYP functionals favored the tetrahedral quartet structure, indicating an energetic preference of the high-spin state with respect to the low-spin one. This effect was more pronounced with the increasing fraction of the Hartree−Fock exchange in the XC functional. On the basis of B3LYP calculations the quartet spin ground state was also predicted for all $Co(acac)_2L_n$ (L = EtOH and H_2O) complexes. The ambiguity of the spin ground state was resolved be means of the temperature-dependent EPR measurements. The characteristic signal observed below 40 K indicates clearly a high-spin quartet state of the $Co(acac)_2(EtOH)_2$ complex. The temperature dependence of the EPR intensity showed a classical Curie−Weiss behavior consistent with the $m_s = \pm 1/2$ Kramers doublet being lower in energy. The pronounced ZFS splitting calculated for the $Co(acac)_2(EtOH)_2$ complex using the CP-B3LYP-SOMF approach can be accounted for by the SOC between α(SOMO) → α(VMO) and β(DOMO) → β(SOMO) states.

AUTHOR INFORMATION

Corresponding Author

*Fax: +48 12 634 05 15. E-mail: pietrzyk@chemia.uj.edu.pl.

ACKNOWLEDGMENT

P.P. and Z.S. acknowledge financial support by the Ministry of Science and Higher Education (MNiSW) of Poland within Grant No. N N204 239334.

REFERENCES

(1) Cotton, F. A.; Elder, R. C. *J. Am. Chem. Soc.* **1964**, *86*, 2294.
(2) Cotton, F. A.; Elder, R. C. *Inorg. Chem.* **1965**, *4*, 1145.
(3) Burgess, J.; Fawcett, J.; Russell, D. R.; Gilani, S. R. *Acta Crystallogr., Sect. C* **2000**, *56*, 649.
(4) Cotton, F. A.; Soderberg, R. H. *Inorg. Chem.* **1964**, *3*, 1.
(5) Debuigne, A.; Caille, J.-R.; Jérôme, R. *Angew. Chem., Int. Ed.* **2005**, *44*, 1101.
(6) Kaneyoshi, H.; Matyjaszewski, K. *Macromolecules* **2006**, *39*, 2757.
(7) Maria, S.; Kaneyoshi, H.; Matyjaszewski, K.; Poli, R. *Chem.—Eur. J.* **2007**, *13*, 2480.

(8) Goto, A.; Fukuda, T. *Prog. Polym. Sci.* **2004**, *29*, 329.
(9) Shmidt, F. K.; Nindakova, L. O.; Shainyan, B. A.; Saraev, V. V.; Chipanina, N. N.; Umanetz, V. A. *J. Mol. Catal. A: Chem.* **2005**, *235*, 161.
(10) Kremer, S.; Henke, W.; Reinen, D. *Inorg. Chem.* **1982**, *21*, 3013.
(11) Sojka, Z.; Witkowski, S. *Top. Catal.* **2002**, *18*, 279.
(12) Vreshch, V. D.; Yang, J.-H.; Zhang, H.; Filatov, A. S.; Dikarev, E. V. *Inorg. Chem.* **2010**, *49*, 8430.
(13) Cotton, F. A.; Holm, R. H. *J. Am. Chem. Soc.* **1960**, *82*, 2979.
(14) Radoń, M.; Srebro, M.; Broclawik, E. *J. Chem. Theory Comput.* **2009**, *5*, 1237.
(15) Ballhausen, C. J. *Introduction to Ligand Field Theory*; McGraw Hill Inc.: New York, 1962.
(16) Frenking, G.; Fröhlich, N. *Chem. Rev.* **2000**, *100*, 717.
(17) Ziegler, T.; Autschbach, J. *Chem. Rev.* **2005**, *105*, 2695.
(18) Jensen, F. *Introduction to Computational Chemistry*, 2nd ed.; John Wiley & Sons: New York, 2006; p 259 and references therein.
(19) Reiher, M.; Salomon, O.; Hess, B. A. *Theor. Chem. Acc.* **2001**, *107*, 48.
(20) Bomble, Y. J.; Vazquez, J.; Kallay, M.; Michauk, C.; Szalay, P. G.; Csaszar, A. G.; Gauss, J.; Stanton, J. F. *J. Chem. Phys.* **2006**, *125*, 064108.
(21) Ye, S.; Neese, F. *Inorg. Chem.* **2010**, *49*, 772.
(22) Neese, F. *Coord. Chem. Rev.* **2009**, *253*, 526.
(23) TeVelde, G.; Bickelhaupt, F. M.; Baerends, E. J.; Fonseca Guerra, C.; van Gisbergen, S. J. A.; Snijders, J. G.; Ziegler, T. *J. Comput. Chem.* **2001**, *22*, 931 and references therein..
(24) Baerends, E. J.; Ellis, D. E.; Ros, P. *Chem. Phys.* **1973**, *2*, 41.
(25) Baerends, E. J.; Ros, P. *Chem. Phys.* **1973**, *2*, 52.
(26) TeVelde, G.; Baerends, E. J. *J. Comput. Phys.* **1992**, *99*, 84.
(27) Fonseca Guerra, C.; Visser, O.; Snijders, J. G.; TeVelde, G.; Baerends, E. J. *Methods and Techniques in Computational Chemistry: METECC-95*; Clementi, E., Corongiu, G., Eds.; STEF: Cagliari, Italy, 1995; p 305.
(28) Becke, A. *Phys. Rev. A* **1988**, *38*, 3098.
(29) Perdew, J. P. *Phys. Rev. B* **1986**, *34*, 7406.
(30) Perdew, J. P. *Phys. Rev. B* **1986**, *33*, 8822.
(31) Lee, C.; Yang, W.; Parr, R. G. *Phys. Rev. B* **1988**, *37*, 785.
(32) Ziegler, T.; Tschinke, V.; Baerends, E. J.; Snijders, J. G.; Ravenek, W. *J. Phys. Chem.* **1989**, *36*, 3050.
(33) Snijders, J. G.; Baerends, E. J. *Mol. Phys.* **1978**, *36*, 1789.
(34) Snijders, J. G.; Baerends, E. J.; Ros, P. *Mol. Phys.* **1979**, *38*, 1909.
(35) Stephens, P. J.; Devlin, F. J.; Chabalowski, C. F.; Frisch, M. J. *J. Phys. Chem.* **1994**, *98*, 11623.
(36) Hertwig, R. H.; Koch, W. *Chem. Phys. Lett.* **1997**, *268*, 345.
(37) Frisch, M. J.; Trucks, G. W.; Schlegel, H. B.; Scuseria, G. E.; Robb, M. A.; Cheeseman, J. R.; Montgomery, J. A., Jr.; Vreven, T.; Kudin, K. N.; Burant, J. C.; Millam, J. M.; Iyengar, S. S.; Tomasi, J. J.; Barone, V.; Mennucci, B.; Cossi, M.; Scalmani, G.; Rega, N.; Petersson, G. A.; Nakatsuji, H.; Hada, M.; Ehara, M.; Toyota, K.; Fukuda, R.; Hasegawa, J.; Ishida, M.; Nakajima, T.; Honda, Y.; Kitao, O.; Nakai, H.; Klene, M.; Li, X.; Knox, J. E.; Hratchian, H. P.; Cross, J. B.; Adamo, C.; Jaramillo, J.; Gomperts, R.; Stratmann, R. E.; Yazyev, O.; Austin, A. J.; Cammi, R.; Pomelli, C.; Ochterski, J. W.; Ayala, P. Y.; Morokuma, K.; Voth, A.; Salvador, P.; Dannenberg, J. J.; Zakrzewski, V. G.; Dapprich, S.; Daniels, A. D.; Strain, M. C.; Farkas, O.; Malick, D. K.; Rabuck, A. D.; Raghavachari, K.; Foresman, J. B.; Ortiz, J. V.; Cui, Q.; Baboul, A. G.; Clifford, S.; Cioslowski, J.; Stefanov, B. B.; Liu, G.; Liashenko, A.; Piskorz, P.; Komaromi, I.; Martin, R. L.; Fox, D. J.; Keith, T.; Al-Laham, M. A.; Peng, C. Y.; Nanayakkara, A.; Challacombe, M.; Gill, P. M. W.; Johnson, B.; Chen, W.; Wong, M. W.; Gonzalez, C.; Pople, J. A. *Gaussian 03*, revision E.01; Gaussian, Inc., Wallingford, CT, 2004.
(38) Schäfer, A.; Huber, C.; Ahlrichs, R. *J. Chem. Phys.* **1994**, *100*, 5829.
(39) Neese, F. *ORCA—An Ab Initio, DFT and Semiempirical Electronic Structure Package*, version 2.6-04.2007; Universität Bonn: Bonn, Germany, 2007.
(40) Neese, F. *J. Chem. Phys.* **2007**, *127*, 164112.
(41) Sinnecker, S.; Neese, F. *J. Phys. Chem. A* **2006**, *110*, 12267.
(42) The low-spin tetrahedral geometry was found unstable converting during the geometry optimization into the square-planar one in agreement with ligand field prediction and Tanabe−Sugano diagrams that indicate only the high-spin state in the whole tetrahedral crystal-field range for the d electron configuration; e.g., see: Drago, R. S. *Physical Methods in Chemistry*; W. B. Saunders Company: Philadelphia, PA, 1977.
(43) Mabbs, F. E.; Collison, D. *Electron Paramagnetic Resonance of d Transition Metal Ions*; Elsevier: Amsterdam, The Netherlands, 1992.
(44) Zarembowitch, J.; Kahn, O. *Inorg. Chem.* **1984**, *23*, 589.
(45) Makinen, M. W.; Kuo, L. C.; Yim, M. B.; Wells, G. B.; Fukuyama, J. M.; Kim, J. E. *J. Am. Chem. Soc.* **1985**, *107*, 5245.
(46) Daul, C.; Schlaepfer, C. W.; von Zelewsky, A. *Struct. Bonding (Berlin)* **1979**, *36*, 129.
(47) Pilbrow, J. R. *Transition Ion Electron Paramagnetic Resonance*; Oxford University Press: New York, U.S.A., 1991.
(48) The assumption is valid in the case of a low concentration of cobalt compound and fulfilling the following energetic condition $|\Delta| > kT \gg h\nu$; see: Weckhuysen, B. M.; Verberckmoes, A. A.; Uytterhoeven, M. G.; Mabbs, F. E.; Collison, D.; de Boer, E.; Schoonheydt, R. A. *J. Phys. Chem. B* **2000**, *104*, 37.
(49) Banci, L.; Bencini, A.; Benelli, C.; Gatteschi, D.; Zanchini, C. *Struct. Bonding (Berlin)* **1982**, *52*, 37.
(50) Krzystek, J.; Ozarowski, A.; Telser, J. *Coord. Chem. Rev.* **2006**, *250*, 2308.
(51) Larrabee, J. A.; Alessi, C. M.; Asiedu, E. T.; Cook, J. O.; Hoerning, K. R.; Klingler, L. J.; Okin, G. S.; Santee, S. G.; Volkert, T. L. *J. Am. Chem. Soc.* **1997**, *119*, 4182.
(52) Sundararajan, M.; Ganyushin, D.; Ye, S.; Neese, F. *Dalton Trans.* **2009**, 6021.
(53) Neese, F. *J. Am. Chem. Soc.* **2006**, *128*, 10213.